**PAPER • OPEN ACCESS**

# High-sensitivity and low-interference gas analyzer with feature extraction from mid-infrared laser absorption-modulated signal

To cite this article: Kyoji Shibuya *et al* 2021 *Meas. Sci. Technol.* **32** 035201

View the article online for updates and enhancements.

# High-sensitivity and low-interference gas analyzer with feature extraction from mid-infrared laser absorption-modulated signal

**Kyoji Shibuya**[1] **, Alexander Podzorov**[2]**, Makoto Matsuhama**[1]**, Katsumi Nishimura**[1] **and Masaaki Magari**[3]

[1] Advanced R&D Center, HORIBA, Ltd., Kyoto, Japan
[2] Automotive Test Systems department, HORIBA FRANCE SAS, Palaiseau, France
[3] Research & Development Division, HORIBA STEC, Co., Ltd., Kyoto, Japan

E-mail: kyoji.shibuya@horiba.com

CrossMark

## Abstract

In this paper, we propose a gas analyzer that uses a quantum cascade laser (QCL) and achieves high sensitivity and gas selectivity with simple configuration and signal processing. Feature quantities are extracted from an absorption-modulated signal, which is obtained by the logarithmic conversion of a detector signal receiving a wavelength-modulated laser light. The extracted feature quantities are used for the determination of target and interfering gas concentration with simple simultaneous linear equations. As a result of the demonstration of CO gas measurement with a gas analyzer consisting of a 4.6 μm pulsed QCL, a small-volume Herriott cell with a path length of 5 m and a thermopile as a photodetector, it is shown that the limit of detection is 2.0 ppb at the integration time of 1 s and that interference by $N_2O$ can be eliminated. It is also shown that various disturbances such as spectral shift due to laser wavelength drift and spectral broadening due to partial pressure change of coexisting gases can be corrected by extracting appropriate additional feature quantities.

Keywords: quantum cascade laser, gas sensing, laser absorption spectroscopy, multi-pass cell, interference correction

(Some figures may appear in colour only in the online journal)

## 1. Introduction

Gas analysis techniques utilizing the infrared absorption characteristics of gas molecules have been used for a long time. One of the most widely used infrared gas analysis techniques is the non-dispersive infrared (NDIR) absorption method using a thermal radiation light source. In this method, the concentration of a target gas is determined from the amount of thermal radiation absorption whose wavelength band is cut out by an optical band-pass filter tailored to the absorption band of the target gas. Because of its simplicity, this method is still used in a wide range of fields such as exhaust gas measurement for automobiles and factories, atmospheric environment monitoring, and process gas control. However, since NDIR only has a wavelength resolution determined by the transmission band of an optical band-pass filter (typically about several tens of wavenumbers), it is difficult to remove the influence of the interfering components in which the absorption bands

overlap. Pneumatic detectors [1–3] have often been used to improve the gas selectivity in NDIR. In pneumatic detectors, a target gas is enclosed in a chamber and a pressure change due to the absorption of intensity-modulated infrared radiation is detected by a microphone or an optical method. The use of pneumatic detectors improves gas selectivity because they are insensitive to infrared absorption other than the absorption band of the enclosed gas. However, when an interfering gas exists in the sample gas whose absorption band overlaps with the target gas, an interference signal appears even for the pneumatic detector. In such a case, the interference can be corrected to some extent when another pneumatic detector in which the interfering gas is enclosed is also used, and the relation of the signals obtained from these two detectors is utilized [4, 5].

Tunable diode laser absorption spectroscopy (TDLAS) has been widely studied as a technique which enables gas analysis with higher sensitivity and lower interference due to higher wavelength resolution and longer optical path length. This is made possible with multi-pass cells and the technique has been applied in industry [6–10]. Initially, TDLAS was developed mainly using near-infrared semiconductor lasers. Subsequently, a mid-infrared semiconductor laser, the quantum cascade laser (QCL), appeared [11]. In recent years, absorption spectroscopy using QCLs has been developed [12–16] because many industrially important gas molecules have strong absorption bands in the mid-infrared region. Our research laboratory has also been focusing on the development of gas analyzers using QCLs [17, 18].

TDLAS and absorption spectroscopy using QCLs can be roughly classified into two methods: direct absorption spectroscopy (DAS) and wavelength modulation spectroscopy (WMS). In DAS, the laser wavelength is swept and an absorbance spectrum is obtained directly from the time waveform of the detector output. In WMS, the laser wavelength is swept at a repetition frequency while modulating the laser wavelength with a small amplitude at a much higher modulation frequency, and a harmonic spectrum is obtained by a lock-in detection of the modulated detector output with harmonics of the modulation frequency. As a result of the lock-in detection, WMS generally has a higher sensitivity than DAS. To enhance the sensitivity even more, multi-harmonic detection schemes were proposed [19]. In this method, the simultaneous curve fitting of multiple harmonic spectra or reconstruction of the transmission spectrum from harmonic coefficients is conducted.

Since DAS can directly obtain an absorbance spectrum, the interference effect of other gases can be removed relatively easily by using linear spectral curve fitting (or a least-squares method). On the other hand, in the case of WMS, it is difficult to remove the interference effect by the linear spectral curve fitting because the linearity of the harmonic spectrum with respect to the concentration is lost. In the case of conventional TDLAS using near-infrared diode lasers, the nonlinearity of the harmonic spectrum is almost negligible because the absorbance is sufficiently small for most gases. In the case of using QCLs, however, the nonlinearity cannot be ignored due to the large absorbance. Therefore, in order to improve the linearity of the harmonic spectrum with respect

to the concentration, a method consisting of taking the logarithm of the detector signal before the lock-in detection has been proposed [20, 21]. In absorption spectroscopy, by taking the logarithm of the detector signal, the output signal can be made linear with respect to concentration according to the Lambert–Beer law. A method combining DAS and WMS by time-division multiplexing has also been proposed [22], which improves the nonlinearity in WMS.

Another method called intra-pulse modulation (IPM) is a unique absorption spectroscopy approach using QCLs [23, 24]. When a QCL is operating in pulsed mode, transient temperature changes in the laser chip cause a wavelength chirp within the pulse duration. This phenomenon allows us to obtain an absorbance spectrum in a single pulse. Since QCLs consume more power than near-infrared diode lasers, a single pulse can produce a larger temperature change, i.e. a larger wavelength change. Typically, a pulse duration of 1 μs produces a wavelength chirp of a few wavenumbers. Although IPM does not require forced wavelength sweeping and allows fast acquisition of the absorption spectrum, it requires a detector and an analog-to-digital converter (ADC) with a sufficiently high response rate. The bandwidth required for the detector and ADC is several hundred MHz to GHz to acquire sub-μs pulse signals with sufficient temporal resolution.

In the methods described above, after obtaining the absorbance spectrum or the harmonic spectrum, the concentration of the target gas is generally calculated by linear or nonlinear spectral curve fitting with model spectra prepared in advance. However, a computer with a high-performance CPU is usually required to perform complex computational processes such as the spectral curve fitting in real time.

For industrial applications, it is important to be able to acquire the absorption signals with cost-effective hardware and to extract desired physicochemical information (gas concentration, temperature, etc) with simpler software (low CPU load) with a lesser error against disturbances such as environmental temperature and pressure changes or interfering gases. Our research laboratory developed a gas analyzer based on IPM [17, 18], but a fast-response MCT detector, a broadband preamplifier and a fast ADC were required. In addition, a bulky computer with a high performance CPU was required to perform complex spectral curve fitting processes in short cycles.

We propose a simpler absorption spectroscopy method, in which the wavelength of the QCL is modulated around an absorption peak of a target gas and the obtained absorption signal is correlated with predetermined feature reference signals (see the detailed explanation below). The idea is similar to the principles of the pneumatic detector type NDIR gas sensor described above and allows effective interference correction in a simple way. We named this method infrared laser absorption modulation (IRLAM) and constructed a gas analyzer using a pulsed QCL, a small volume multi-pass cell and a thermopile to demonstrate this method. All of these components are manufactured in house. This method does not require a fast-response detector nor an ADC as in IPM and can demonstrate sufficient performance even when using an inexpensive thermopile as a thermal detector. Since this technique is similar in principle to the pneumatic detector-type NDIR, it can also
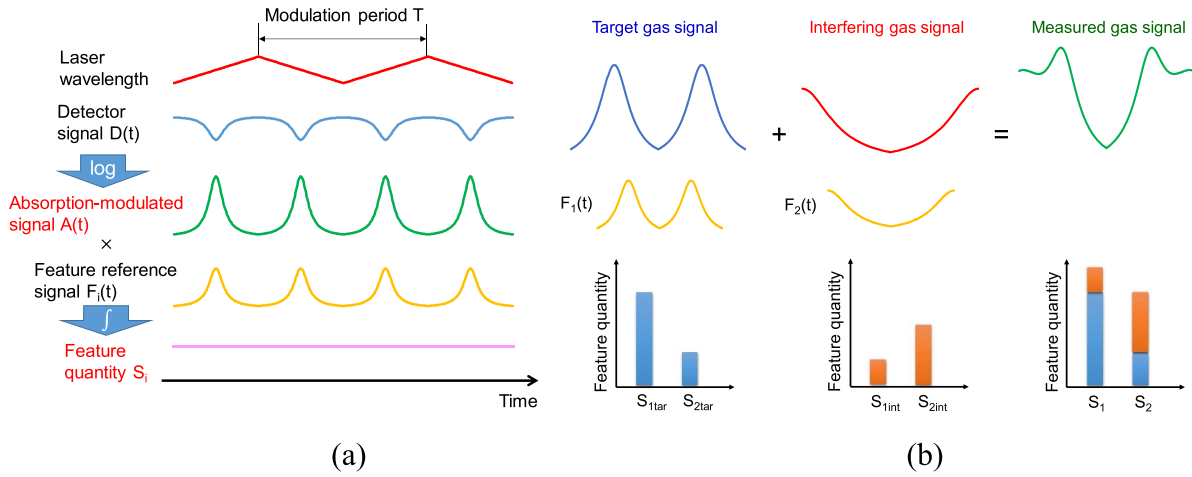
**Figure 1.** Conceptual diagram of the measurement principle of IRLAM for (a) the feature quantity extraction and (b) the interference correction.

be called 'Advanced NDIR'. The details of this method and the results of the demonstrations are described below.

## 2. Principle

The output from a pneumatic detector $V_{\text{out}}$ is proportional to the correlation of the absorption spectrum of the enclosed gas $D(\lambda)$ and the power spectrum of the light source $I(\lambda)$ as shown in the following equation:

$$V_{\text{out}} \propto \int I(\lambda) \cdot D(\lambda) \, d\lambda. \tag{1}$$

That is, if there is no overlap between the power spectrum of the light source and the absorption spectrum of the pneumatic detector, the output signal is null. This offers some degree of gas selectivity, but the output signal is affected when the absorption spectrum of an interfering gas overlaps with that of the pneumatic detector. In order to improve such a situation, two pneumatic detectors in which a target gas and an interfering gas are enclosed respectively are prepared. The interference can be corrected by using the relationship between two output signals from the pneumatic detectors. As an analogy to this idea, we devised a method of the interference correction using 'feature quantities' (adopting the image processing vocabulary) which are extracted from the time domain absorption-modulated signal by correlating it with several reference signals prepared in advance (referred to as 'feature reference signals' below). In this case, it is not necessary to prepare several detectors and, instead, only several feature reference signals have to be prepared in the software.

Figure 1 shows a conceptual diagram of the measuring principle of IRLAM. When the wavelength of a QCL is modulated around a peak of the absorption spectrum of a target gas, the detector output signal $D(t)$ changes according to the shape of the absorption spectrum of a sample gas. Then, as shown in (2), the absorption-modulated signal for the sample gas, $A(t)$, is given by taking the logarithm of $D(t)$ and removing the DC component, and the feature quantities for the sample gas, $S_i$, are obtained by correlating $A(t)$ with the feature reference signals $F_i(t)$ ($i = 1, 2,.., n$, where $n$ is a positive integer) in the modulation period $T$. Removing the DC component makes the absorption-modulated signal insensitive to light intensity changes. Even when there is no absorption at a zero gas, the absorption-modulated signal has a shape according to the laser intensity variation due to the drive current modulation. Therefore, the feature quantities for zero gas are not null and it is needed to subtract their contributions. When the absorption-modulated signal and feature quantities for the reference gas or zero gas are expressed as $A_0(t)$ and $R_i$, respectively, the differences between $S_i$ and $R_i$ are defined as zero-calibrated feature quantities $S_i'$:

$$S_i = \int_{-T/2}^{T/2} A(t) \cdot F_i(t) \, dt,$$

$$-A(t) = \ln D(t) - \frac{1}{T} \int_{-T/2}^{T/2} \ln D(t) \, dt,$$

$$R_i = \int_{-T/2}^{T/2} A_0(t) \cdot F_i(t) \, dt,$$

$$-A_0(t) = \ln D_0(t) - \frac{1}{T} \int_{-T/2}^{T/2} \ln D_0(t) \, dt,$$

$$S_i' = S_i - R_i. \tag{2}$$

$F_i(t)$ can be set to arbitrary functions according to the features to be extracted from the absorption-modulated signal $A(t)$. Larger feature quantities can be obtained by setting these functions close to the shape of the absorption-modulated signal of the target or interfering gas. A system of functions based on Lorentzian profiles or Voigt profiles is suitable for the feature reference signals, and each feature reference signal can be a function made orthogonal to the others, for example, by using the Gram–Schmidt orthogonalization procedure. Considering the analogy with the NDIR techniques, $A(t)$, $F_i(t)$ and $S_i$ correspond to the power spectrum of the light transmitted through the sample gas, the absorption spectra having each pneumatic detector and the output signals obtained from each pneumatic detector, respectively.

The zero-calibrated feature quantities $S_i'$ obtained as described above are given by a linear combination of the concentrations of the respective gases due to the linearity and independence of the absorption-modulated signal with respect to the concentrations as shown in figure 1(b). This linearity and independence facilitate the accurate determination of the concentration of the target gas while correcting the influence of the interfering gas. For example, assuming one target gas and one interfering gas, if two feature reference signals $F_1(t)$ and $F_2(t)$ are prepared and the zero-calibrated feature quantities $S_1'$ and $S_2'$ are obtained from the sample measurement, the target gas concentration $C_{tar}$ and the interfering gas concentration $C_{int}$ are coupled to $S_1'$ and $S_2'$ by simple linear relationships as follows:

$$s_{1tar}C_{tar} + s_{1int}C_{int} = S_1'$$
$$s_{2tar}C_{tar} + s_{2int}C_{int} = S_2', \tag{3}$$

where $s_{1tar}$ and $s_{2tar}$ are the zero-calibrated feature quantities per unit concentration of the target gas for respective feature reference signals, and $s_{1int}$ and $s_{2int}$ are those of the interfering gas. These parameters are obtained before the sample measurement. Only by solving these linear simultaneous linear equations, is it possible to determine the target gas concentration $C_{tar}$ from which the influence of the interfering gas is removed. Furthermore, even when two or more interfering gas components are present, the target gas concentration with interference correction can be obtained by adding different feature signals and solving simultaneous linear equations whose number is equal to the number of gas components. Generally, when $n$ kinds of gases including the target and interfering gases are present, the zero-calibrated feature quantity per unit concentration for the $i$th feature reference signal $F_i(t)$ of the $j$th gas component is defined as $s_{ij}$ and the concentration of the $j$th gas component is defined as $C_j$, the following simultaneous linear equations are obtained:

$$s_{11}C_1 + s_{12}C_2 + s_{13}C_3 + \ldots + s_{1n}C_n = S_1'$$
$$s_{21}C_1 + s_{22}C_2 + s_{23}C_3 + \ldots + s_{2n}C_n = S_2'$$
$$s_{31}C_1 + s_{32}C_2 + s_{33}C_3 + \ldots + s_{3n}C_n = S_3' \tag{4}$$
$$\vdots$$
$$s_{n1}C_1 + s_{n2}C_2 + s_{n3}C_3 + \ldots + s_{nn}C_n = S_n'.$$

Alternatively, the concentration of each gas may be determined by the least-squares method with further adding linear equations formed by additional different feature quantities. This makes it possible to determine the concentration by reducing the error due to the measurement noise.

Thus, the IRLAM method can offer a simple and powerful interference correction scheme with fewer variables than conventional spectral curve-fitting processes by compressing spectral information with the feature extraction. For typical spectral curve fitting, several hundreds of simultaneous linear equations are needed because of several hundreds of spectral data points. In the case of the IRLAM method, however, since the number of the simultaneous linear equations is at most around 10, the calculation time can be expected to be reduced by a factor 10–100. Therefore, even when a fast-response

real-time measurement is required, a high-performance computer is not necessary and an embedded processor is enough. This makes it possible to construct an analyzer without a bulky computer system, which is greatly beneficial for industrial applications.

In conventional TDLAS, the relation between time and wavelength is obtained in advance, the absorption signal is converted into an absorption spectrum and the curve-fitting calculation is performed with model spectra prepared based on a spectrum database such as HITRAN [25]. In contrast, in the IRLAM method, the zero-calibrated feature quantities per unit concentration of the target and interfering gas, $s_{ij}$, are recorded in advance with real gases at known concentrations instead of model spectra in a database. This eliminates the need for time-to-wavelength conversion required by conventional spectral curve fitting and enables measurement of gases for which no spectral data exist in databases such as HITRAN.

In addition, not only the influence of interfering gases, but also various disturbances affecting measurement results such as a laser wavelength shift due to environmental temperature change and spectral broadening due to changes in the partial pressure of the coexisting gases can be corrected by a simple calculation process using the relationships between the feature quantities.

## 3. Experimental setup

In order to demonstrate the measurement principle described above, an analyzer as shown in figure 2 was constructed. A single-mode pulsed QCL operating at the wavelength of 4.6 μm was used as a laser source, a thermopile was used as a photodetector and a Herriott cell [26] having an optical path length 5 m was used as a gas cell. The target gas of this analyzer was CO. By using the pulsed QCL, the power consumption was further reduced and waste heat treatment was facilitated. The QCL, the Herriott cell and the thermopile were all manufactured in-house by HORIBA, Ltd. (Kyoto, Japan). The optical output of the in-house QCL used in this experiment was about 100 mW of pulse peak power. The photosensitive area of the thermopile was 0.75 mm$^2$ and the detectivity ($D*$) was $1.3 \times 10^8$ cm√Hz/W. The output signal of the thermopile was amplified and acquired by a data acquisition board with a 24 bit ADC at the sampling rate of 10 kHz. The sample gas was introduced to the Herriott cell with a flow rate of $2\,l\,min^{-1}$ after conditioning with standard gas cylinders and mass flow controllers. The temperature and pressure in the cell were set to be room temperature and atmospheric pressure, respectively (not controlled).

As shown in figure 3, the Herriott cell is designed so that the reflected beams lie on one plane, and the spherical mirrors are cut in order to reduce the cell volume as much as possible and improve the gas replacement speed. The mirror surface is coated with gold, so that the reflectivity in the mid-infrared range and the corrosion resistance are improved. The optical path length of 5 m with an internal volume of only about 40 ml is realized by making the beam reflect itself 50 times between the mirrors set 100 mm apart.
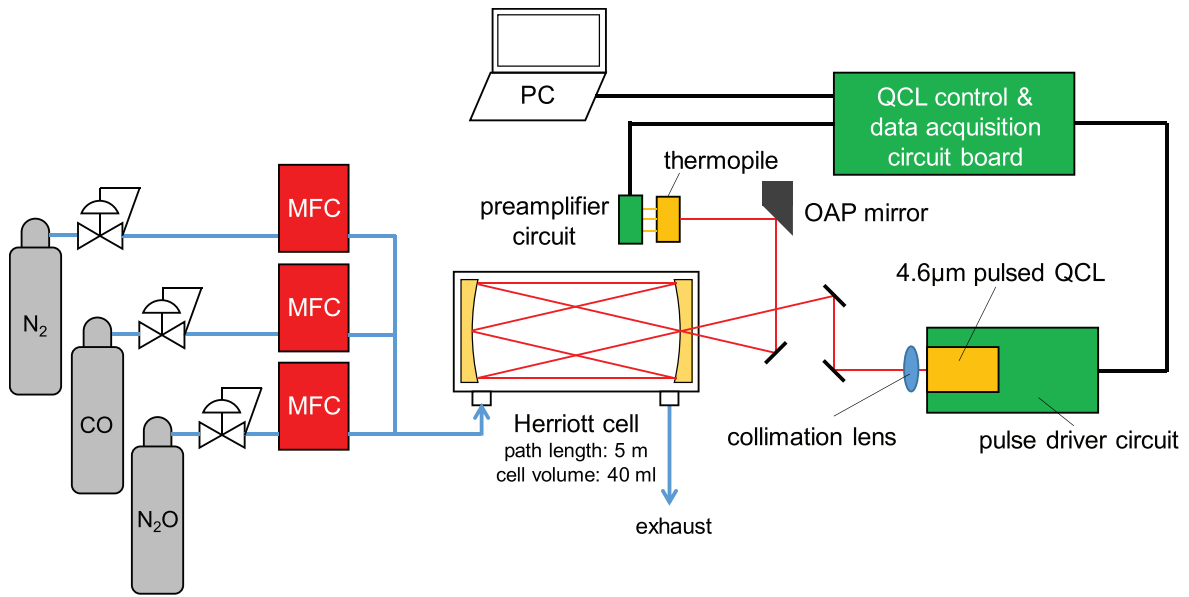
**Figure 2.** IRLAM gas analyzer configuration and the experimental setup.
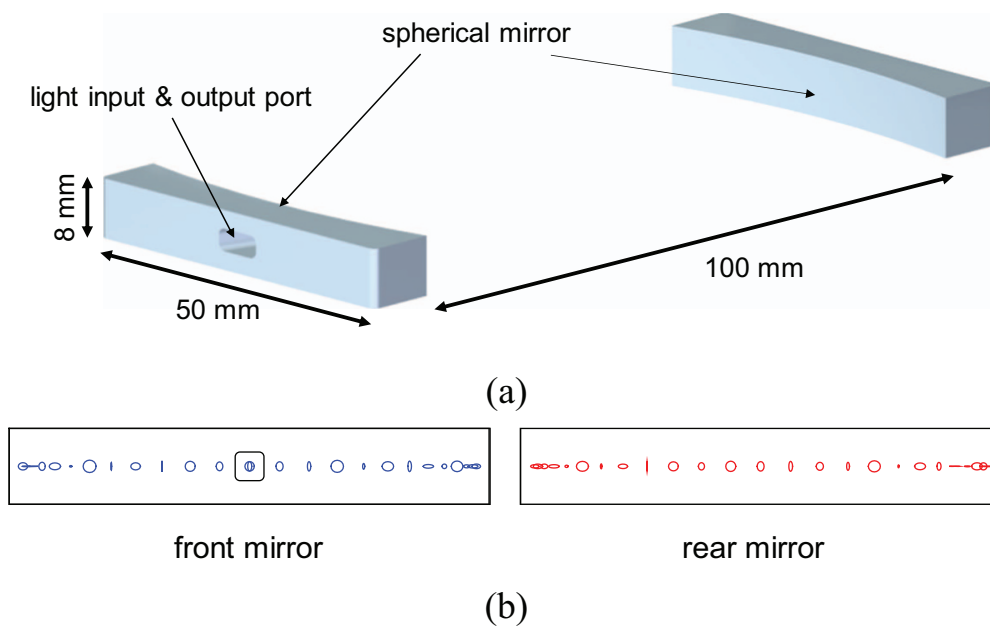


**Figure 3.** (a) Mirror configuration for the small-volume Herriott cell with 5 m pathlength and (b) its beam spots on the mirrors (the beam spots are calculated with a homemade ray optics simulator written in Mathematica).

Figure 4(a) shows light output power–current–voltage (L-I-V) characteristics of the pulsed QCL manufactured by ourselves. The active layer of the QCL is composed with InGaAs/InAlAs quantum well/barriers grown by metal–organic vapor phase epitaxy. The input voltage applied to the QCL was controlled as shown in figure 4(b). If the pulse repetition period is sufficiently shorter than the response time of the detector, the signal of the pulse train is averaged and approximately the same as that of the continuous-wave (CW) operation. Therefore, such an operation is often referred to as a quasi-CW operation [27]. In the quasi-CW operation, the shorter the pulse width, the higher the wavelength resolution,

and the higher the duty ratio, the higher the signal intensity. In the present experiment, the pulse width and duty ratio were set to 10 ns and 5%, respectively. In addition, in order to modulate the QCL wavelength, a modulation voltage was superimposed at below the oscillation threshold voltage $V_{th}$ with keeping the pulse oscillation voltage constant. The modulation frequency was set to 10 Hz in consideration of the response speed of the thermopile used as a detector. The modulation voltage requires a certain offset voltage because of the current–voltage characteristics of the QCL (almost no current flows in the vicinity of 0 V as shown in figure 4(a)). In this experiment, the modulation voltage was set to an amplitude ($V_{amp}$) of 0.8 V
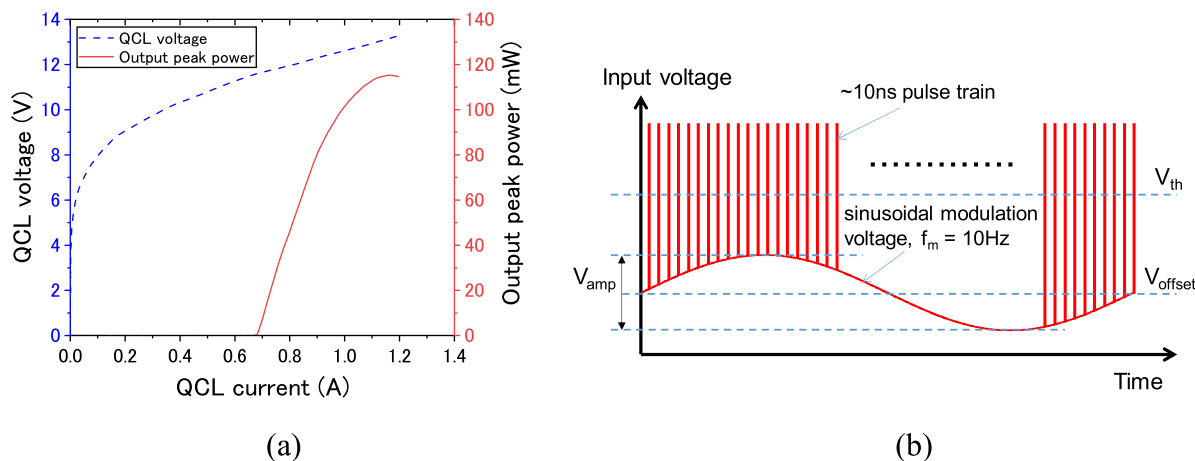
(a)                                        (b)

**Figure 4.** (a) Light output power–current–voltage characteristics of the in-house pulsed QCL and (b) schematic of the drive condition for the quasi-CW operation with the pulsed QCL.
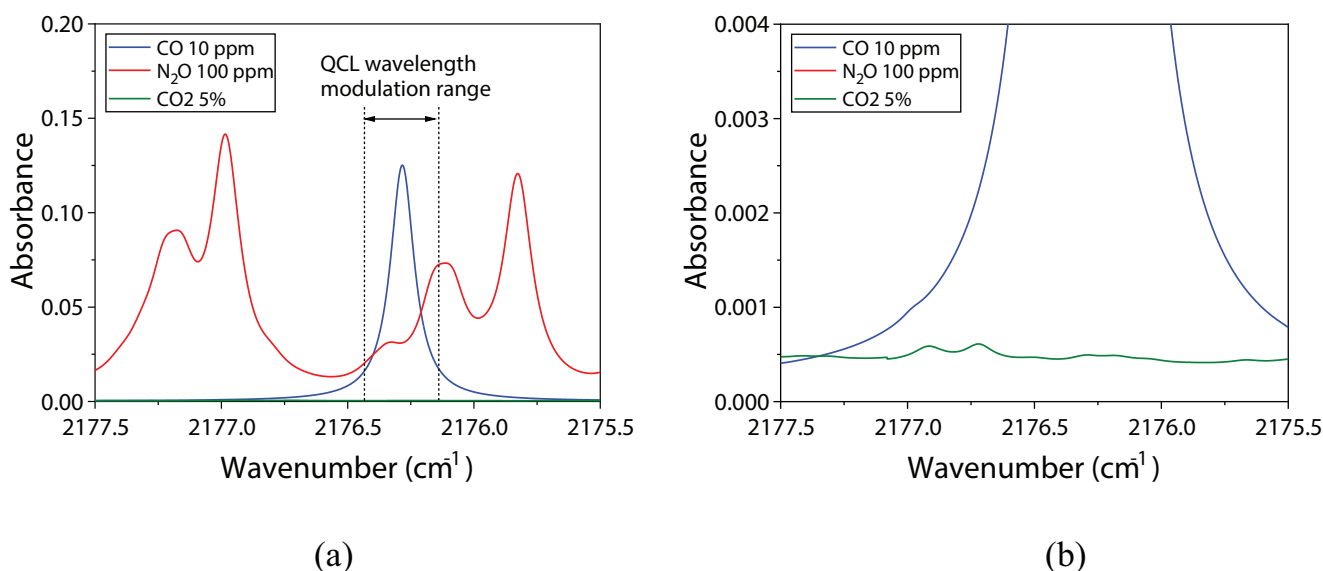


(a)                                        (b)

**Figure 5.** (a) CO, $N_2O$ and $CO_2$ absorption spectra in the QCL operating wavenumber range and (b) its enlarged view (the spectra are calculated from the HITRAN database [25] at 300 K and 1 atm).

with an offset ($V_{offset}$) of 6.2 V in order to obtain the necessary modulation depth. The oscillation threshold voltage ($V_{th}$) was about 11.5 V.

The calculated absorption spectra of 10 ppm of CO as the target component and 100 ppm of $N_2O$ and 5% of $CO_2$ as interfering components in the QCL operating wavelength range are shown in figure 5. It is expected from these spectral features that the interference from $N_2O$ is considerably large while that from $CO_2$ is almost negligible. We demonstrated how the interference correction of IRLAM works in these conditions.

## 4. Experimental results and discussions

The results of the demonstration of the IRLAM method using the above experimental setup are described below. Figure 6 shows examples of the absorption-modulated signals and the feature quantities extracted in this experiment. These signals are obtained by aligning the center of the QCL wavelength

range with the absorption peak of CO and modulating the wavelength to reach the tail of the absorption spectrum as shown in figure 5(a). The signal acquisition and concentration calculations are performed in every modulation cycle of 100 ms.

Figure 6(a) shows the absorption-modulated signals obtained by taking the logarithm of the detector signals when the zero gas, the target gas and the interfering gas are flowing, respectively. In addition, two feature reference signals chosen in order to extract the feature quantities from the absorption-modulated signals are also shown in figure 6(a). The feature reference signals are set to Lorentzian profiles according to the spectrum shapes of the target and interfering gas. For the target gas, since the wavelength modulation goes back-and-forth around the peak of the absorption spectrum, the absorption-modulated signal and the feature signal have two peaks in one modulation period, whereas for the interfering gas, since the wavelength modulation goes back-and-forth only over the
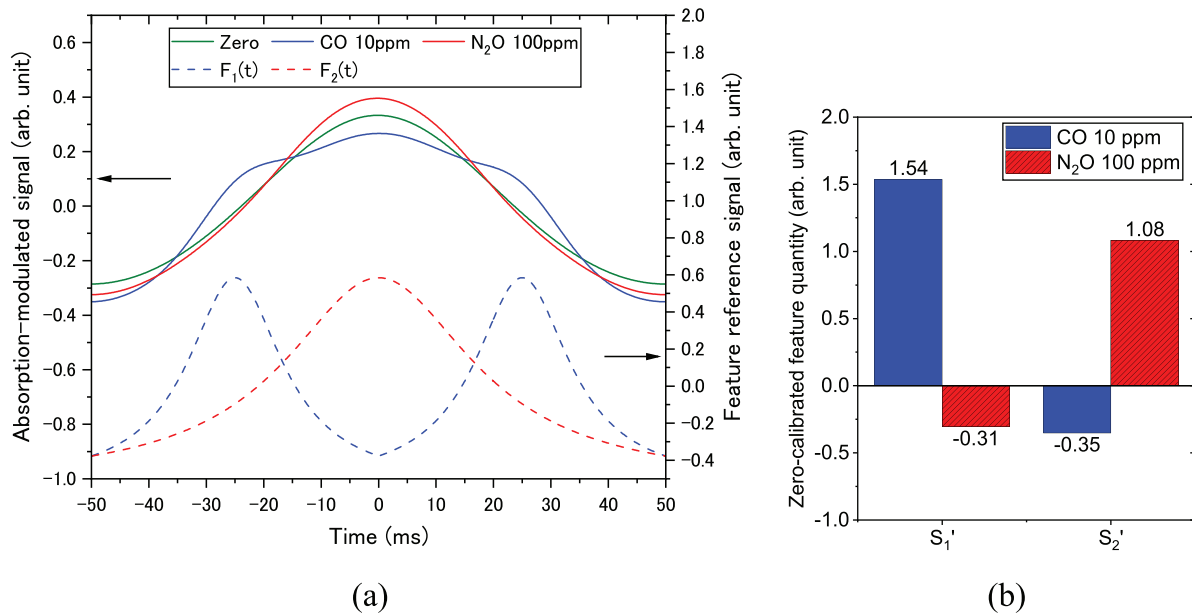
**Figure 6.** Time waveforms of (a) the absorption-modulated signals (solid lines), the feature reference signals (dotted lines), and (b) the zero-calibrated feature quantities obtained from them, when each gas is introduced into the gas cell.

slope of the absorption spectrum, they have only one peak in one modulation period.

Figure 6(b) shows the feature quantities extracted by correlating the absorption-modulated signals with the feature reference signals. From figure 6(b), it can be seen that the balances of the zero-calibrated feature quantities for the respective gases are different and the $S_1'$ is a dominant component for CO gas, whereas the $S_2'$ is a dominant component for N$_2$O gas. Since these $S_1'$, $S_2'$ are linear with respect to the concentration, and the ratio of $S_1'$ and $S_2'$ differs for each gas, the concentration of the target and interfering gas can be determined separately by solving the simultaneous linear equations as shown in (3). In order to make this measurement in practice, calibration processes are needed in advance using the zero, target and interfering gases of a known concentration to obtain $s_{ij}$, which is the zero-calibrated feature quantity per unit concentration for each gas and feature reference signal.

Figure 7(a) shows a plot of the zero-calibrated feature quantities $S_1'$ and $S_2'$ against the concentration of the CO gas introduced into the gas cell at concentrations from 0 to 10 ppm. It can be confirmed that the feature quantity has a good linearity with respect to the concentration. This comes from the characteristic of the absorption-modulated signal, which is a logarithm of the detector signal. Moreover, figure 7(b) shows additional linearity test results with 10–200 ppm CO gas to examine the range in which the linearity is maintained. In figure 7(b) it is shown that the deviation from the linear fit of 0–10 ppm increases gradually over 10 ppm and the deviation is over 5% and 10% when the feature quantity reaches 7.3 at 50 ppm and 13.8 at 100 ppm, respectively. The peak absorbance of CO gas at 100 ppm is 1.2 as estimated from figure 5. We believe that the limitation of the linearity mainly comes from lower spectral resolution in the quasi-cw operation. In the quasi-cw operation the wavelength chirp in

the laser pulse is averaged. This degrades the spectral resolution in the absorption-modulated signal. The linearity may be improved if a shorter pulse operation or a cw operation is introduced.

The results of the demonstration of the interference correction are described next. Figure 8 shows concentration values calculated based on the extracted feature quantities when CO 10 ppm as a target component and N$_2$O 100 ppm as an interfering component are sequentially introduced into the gas cell. An enlarged plot near zero over a time span of 0–300 s is also shown in figure 8(b) to confirm the noise level. The blue line shows concentration values calculated with $S_1'$ only, while the red line shows concentration values calculated with $S_1'$ and $S_2'$ based on (3). The measurement uncertainty of CO concentration is 6.5 ppb; it is defined as the standard deviation of the measurement results in the time range from 0 to 50 s in figure 8(b). On the blue line, a negative interfering effect appears when N$_2$O 100 ppm is introduced. This is because the negative zero-calibrated feature quantity $S_1'$ of N$_2$O, as shown in figure 6(b), directly affects the concentration values. On the other hand, on the red line, it is found that the interfering effect of N$_2$O is almost completely eliminated by the interference correction scheme of IRLAM. The rise and fall response time (10%–90%) are 1.3 s and 1.0 s from figures 8(c)–(d), respectively. These response times are almost identical to the gas replacement time for 40 ml volume with a 2 l min$^{-1}$ flow rate.

The limit of detection (LOD) of CO was estimated from the results of figure 8. When the LOD is defined as the standard deviation of the read-out concentration values at zero gas, it is 6.5 ppb for 0.1 s integration and 2.0 ppb for 1 s integration. Figure 9 shows the experimental result of the Allan deviation plot. The LOD is improved to 0.45 ppb when integrating for 30 s. In [28] it was reported that the LOD is 1.4 ppb for 1 s
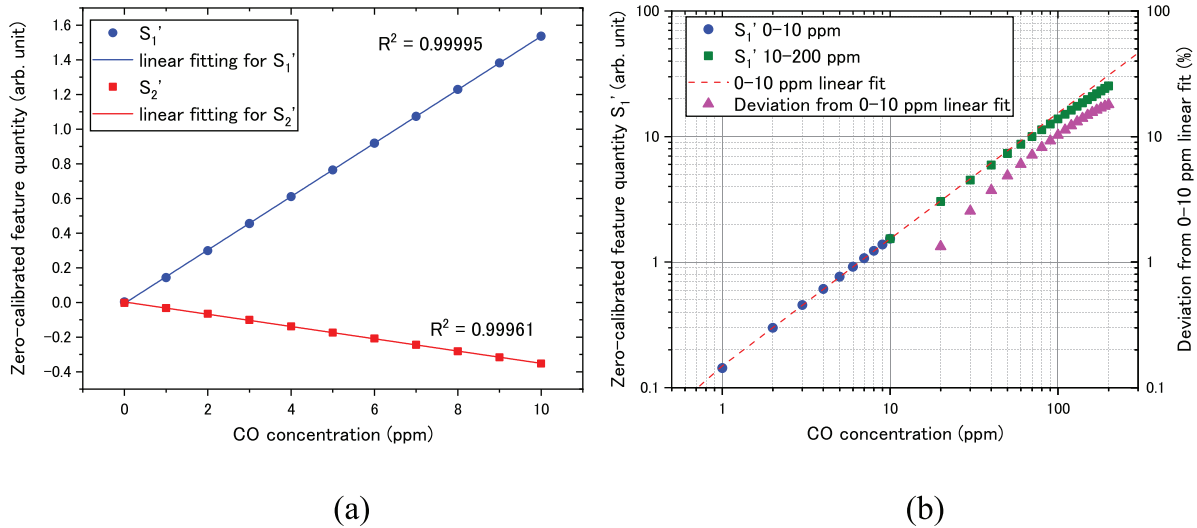
(a)



(b)

**Figure 7.** Linearity of the zero-calibrated feature quantity to CO concentration in (a) 0–10 ppm and (b) 0–200 ppm ranges.
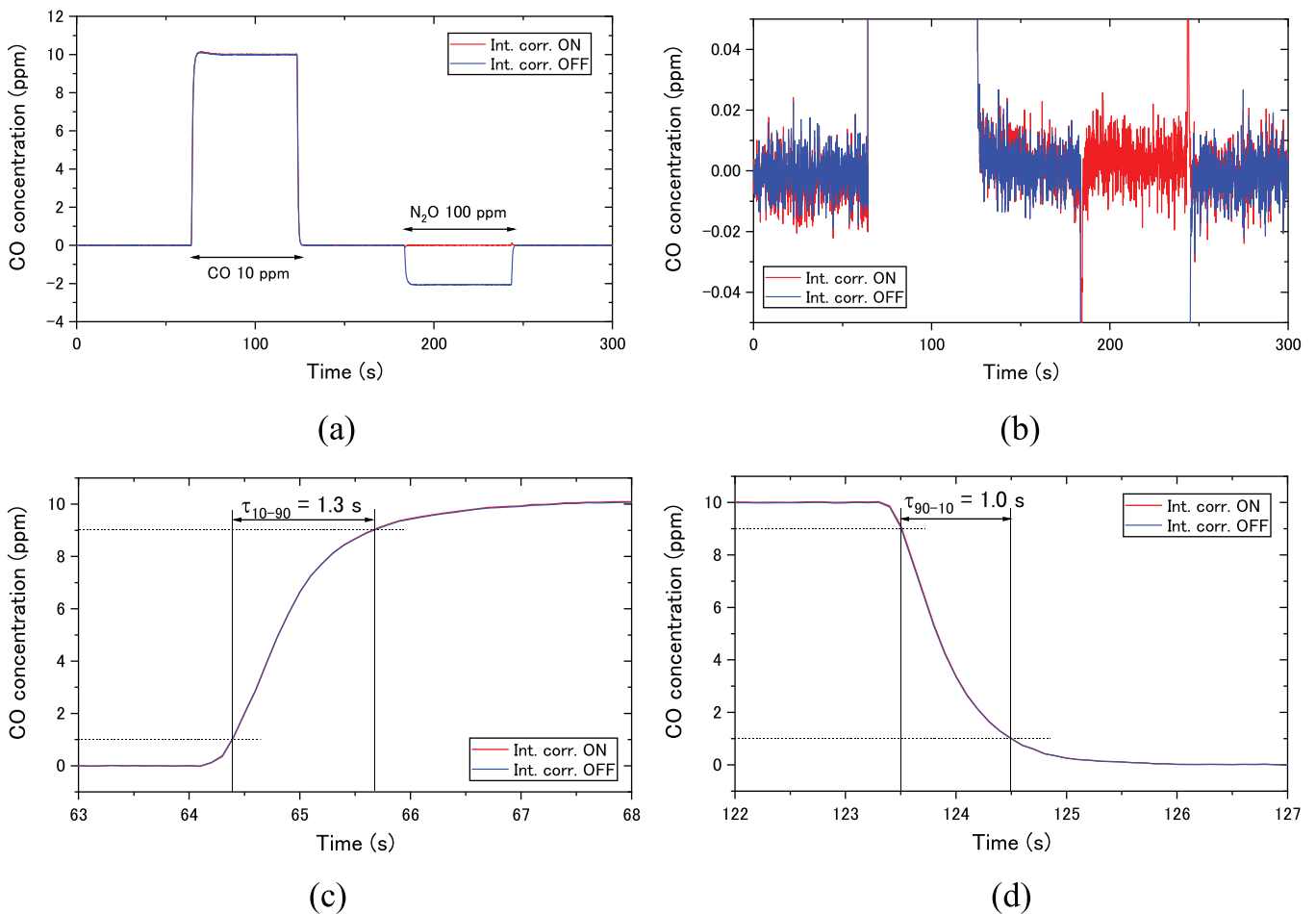


(a)



(b)



(c)



(d)

**Figure 8.** (a) Results of the measurement of CO when the interference correction for $N_2O$ is active (red line) and inactive (blue line) and its enlarged view around (b) zero concentration, (c) rise response and (d) fall response.

integration and 0.28 ppb for 50 s integration using a cw-QCL-based WMS with a 36 m Herriott cell and a thermoelectrically cooled MCT detector in the same wavelength region. The IRLAM analyzer could show a similar LOD even though the

configuration with a 5 m Herriott cell and a thermopile was used.

Although the solution can in principle be obtained if there are at least two feature quantities for two unknowns, in order
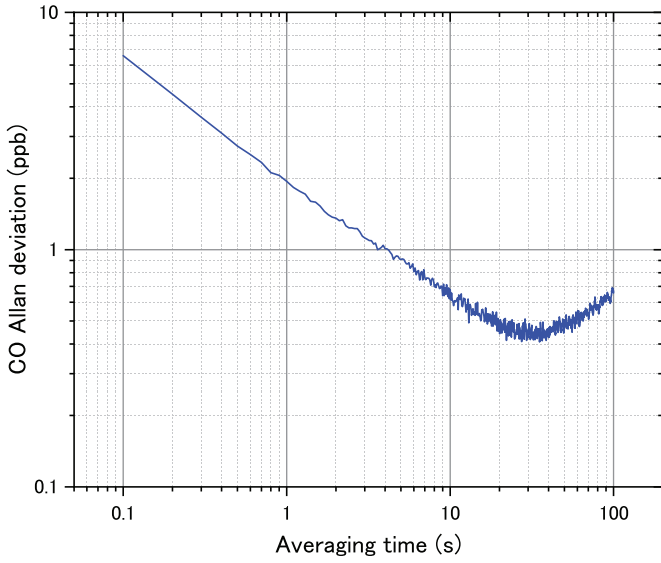
**Figure 9.** Allan deviation plot for the CO measurement with the IRLAM analyzer.

to suppress the influence of various disturbance factors and noises, it is possible to obtain a more robust result by increasing the number of feature quantities to about 5–10 and obtaining the solution by the least-squares method. For example, as the feature reference signals to be added, signals that can capture a spectral broadening due to partial pressure change of coexisting gases or a spectral shift due to a drift in the laser wavelength can be considered. If such feature quantities can also be extracted, disturbances such as the spectral broadening or the spectral shift can also be corrected. For this purpose, four feature reference signals $F_1(t)$, $F_2(t)$, $F_3(t)$ and $F_4(t)$ based on Lorentzian functions as shown in (5) may be used as an example. $F_1(t)$ and $F_2(t)$ are used to capture the absorption spectrum shapes of the target and interfering gases with their Lorentzian profiles. $F_3(t)$ and $F_4(t)$ are expressed as partial derivatives of the Lorentzian function with the time shift $t_a$ and the Lorentzian width $w_a$ to capture the spectral shift and the spectral broadening; these feature reference signals are offset so that the integrals of one modulation period are 0:

$$F_1(t) = \frac{A_1}{1 + \left(\frac{|t| - t_a}{w_a}\right)^2} - B_1 \left(-\frac{T}{2} \leqslant t < \frac{T}{2}\right),$$

$$F_2(t) = \frac{A_2}{1 + \left(\frac{|t| - t_b}{w_b}\right)^2} - B_2 \left(-\frac{T}{2} \leqslant t < \frac{T}{2}\right),$$

$$F_3(t) = \frac{A_3}{A_1}\frac{\partial F_1}{\partial t_a} - B_3 = \frac{2A_3(|t| - t_a)}{w_a^2\left(1 + \left(\frac{|t| - t_a}{w_a}\right)^2\right)^2} - B_3,$$

$$F_4(t) = \frac{A_4}{A_1}\frac{\partial F_1}{\partial w_a} - B_4 = \frac{2A_4(|t| - t_a)^2}{w_a^3\left(1 + \left(\frac{|t| - t_a}{w_a}\right)^2\right)^2} - B_4, \quad (5)$$

where $A_1$, $A_2$, $A_3$ and $A_4$ are constants and $B_1$, $B_2$, $B_3$ and $B_4$ are offsets to make zero the integrals of $F_1(t)$, $F_2(t)$, $F_3(t)$ and $F_4(t)$ in one modulation period $T$, respectively. If the gas absorption spectrum is expressed as a Lorentzian function, the maximum feature quantities can be extracted from the absorption-modulated signal when using the Lorentzian-based feature reference signals $F_1(t)$ and $F_2(t)$. Since the absorption-modulated signal is folded back in half of the modulation period $T$, the feature reference signal also changes that way. Therefore, $F_1(t)$ and $F_2(t)$ are expressed as functions of $|t|$. When using the partial derivative of $F_1(t)$ with respect to the time shift $t_a$, $F_3(t)$, this feature reference signal is sensitive to the shift in the absorption spectrum of the target gas due to the laser wavelength drift. In the same manner, when using the partial derivative of $F_1(t)$ with respect to the Lorentzian width $w_a$, $F_4(t)$, this feature reference signal is sensitive to the change in the absorption spectrum width of the target gas due to the spectral broadening. With these feature reference signals, it is possible to extract the feature quantities for correcting the interference, the spectral shift and the spectral broadening. Furthermore, these feature reference signals can be made orthogonal to each other. When using the orthogonal feature reference signal set, each extracted feature quantity is independent of each other. This allows for more effective feature extraction from the absorption-modulated signal. In this case, for example, the above four feature reference signals can be converted into orthogonalized feature reference signals, $G_1(t)$, $G_2(t)$, $G_3(t)$ and $G_4(t)$, using the Gram–Schmidt orthogonalization procedure shown in (6). Figures 10(a)–(b) show the feature reference signals expressed as (5) and (6), respectively when $T = 100$ ms, $t_a = 25$ ms, $w_a = 10$ ms, $t_b = 0$ ms and $w_b = 20$ ms:

$$G_1(t) = F_1(t),$$

$$G_2(t) = F_2(t) - \frac{\int_{-T/2}^{T/2} G_1(t) F_2(t) \, dx}{\int_{-T/2}^{T/2} G_1(t) G_1(t) \, dx} G_1(t),$$

$$G_3(t) = F_3(t) - \frac{\int_{-T/2}^{T/2} G_1(t) F_3(t) \, dx}{\int_{-T/2}^{T/2} G_1(t) G_1(t) \, dx} G_1(t)$$
$$- \frac{\int_{-T/2}^{T/2} G_2(t) F_3(t) \, dx}{\int_{-T/2}^{T/2} G_2(t) G_2(t) \, dx} G_2(t),$$

$$G_4(t) = F_4(t) - \frac{\int_{-T/2}^{T/2} G_1(t) F_4(t) \, dx}{\int_{-T/2}^{T/2} G_1(t) G_1(t) \, dx} G_1(t)$$
$$- \frac{\int_{-T/2}^{T/2} G_2(t) F_4(t) \, dx}{\int_{-T/2}^{T/2} G_2(t) G_2(t) \, dx} G_2(t)$$
$$- \frac{\int_{-T/2}^{T/2} G_3(t) F_4(t) \, dx}{\int_{-T/2}^{T/2} G_3(t) G_3(t) \, dx} G_3(t). \quad (6)$$
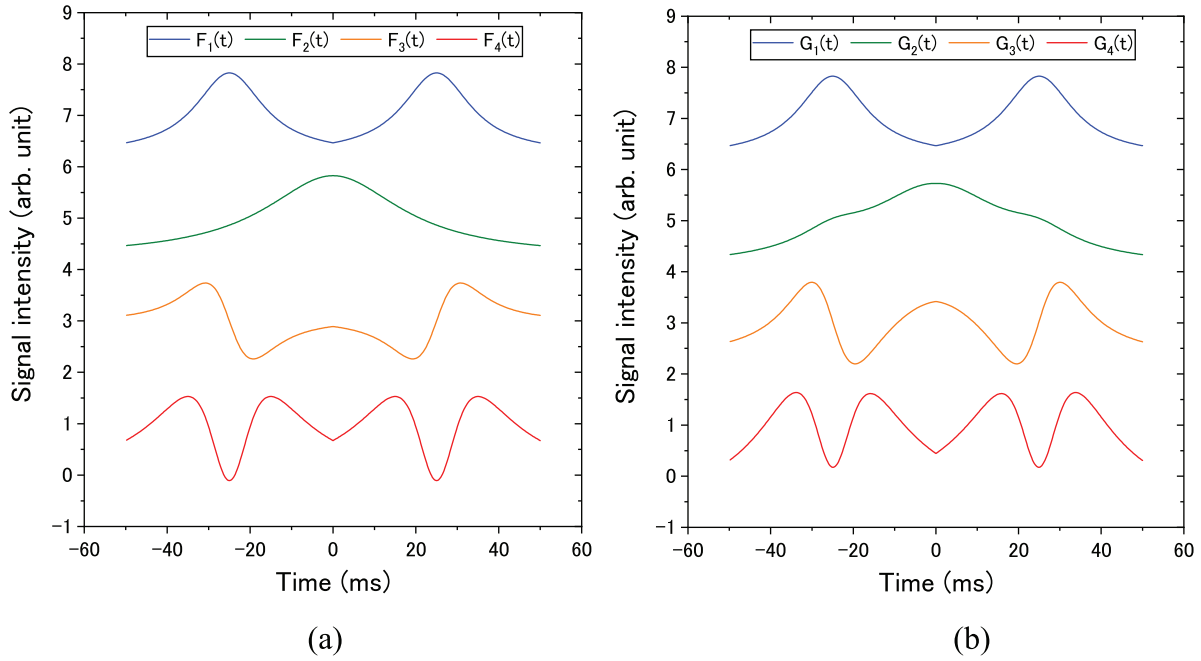
(a)

(b)

**Figure 10.** (a) Examples of feature reference signals and (b) their orthogonalized signals with the Gram–Schmidt conversion (each plot is offset for clarity).
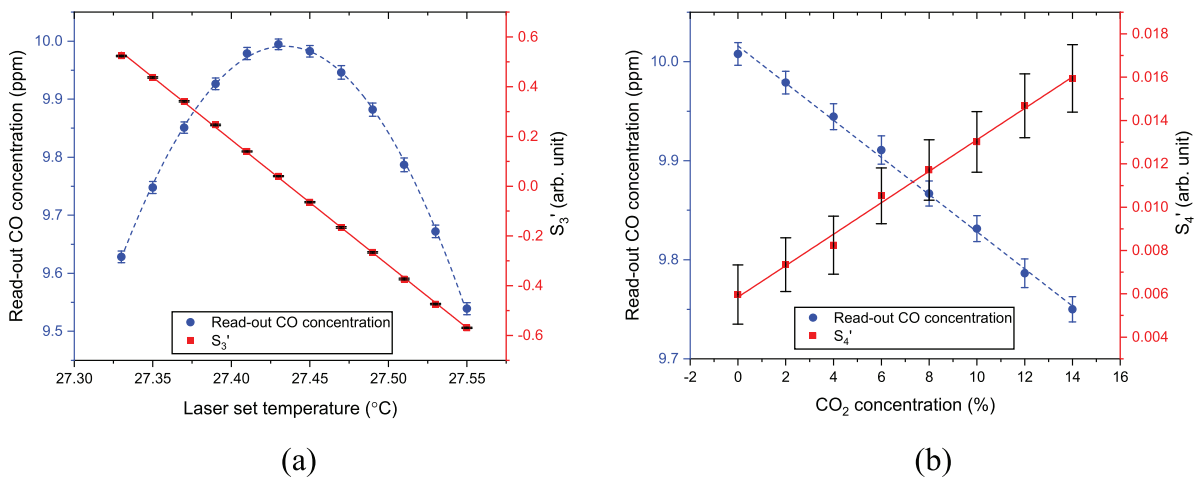


(a)

(b)

**Figure 11.** Changes in the feature quantities and the read-out concentration value for (a) the laser wavelength shift and (b) the spectral broadening. The error bars represent the standard deviations.

It was assessed how the spectral broadening due to coexisting gases and the laser wavelength shift can be captured by the feature quantities extracted using these feature reference signals. Figure 11(a) shows the plots of the zero-calibrated feature quantity $S_3'$ extracted with $G_3(t)$ depending on the laser wavelength shift and of the read-out CO concentration based on $S_1'$ when the laser temperature was being changed to generate the wavelength shift. In this measurement, CO concentration in the cell was kept constant at 10 ppm. The wavelength shift feature quantity $S_3'$ changes linearly with the laser temperature change, while the read-out concentration value has a maximum value at some laser temperature. Also, figure 11(b) shows the plots of the zero-calibrated feature quantity $S_4'$ extracted with $G_4(t)$ depending on the

spectral broadening and the read-out CO concentration based on $S_1'$ when the concentration of $CO_2$, the coexisting gas, was being changed. The read-out CO concentration decreases with increasing $CO_2$ concentration, even though the $CO_2$ absorption in this wavelength modulation range is almost negligible, as shown in figure 5(b). This comes from the fact that the height of the absorption peak was reduced by the spectral broadening due to the change of the coexisting gas partial pressure. On the other hand, the spectral broadening feature quantity $S_4'$ increases with increasing $CO_2$ concentration. This comes from the fact that $S_4'$ has a positive sensitivity to the increase of the spectral width. These two feature quantities $S_3'$ and $S_4'$ can be used as indicators to detect and correct the wavelength shift and the spectral broadening. Comparing the

error bars of $S_3{}'$ and $S_4{}'$ in figures 11(a)–(b), it is found that the laser wavelength shift can be detected more sensitively than the spectral broadening. This means that the change in spectral shape due to the wavelength shift is easy to distinguish from that due to the concentration change, whereas the change in spectral shape due to the spectral broadening is hard to distinguish from that due to the concentration change. Thus, when introducing additional feature quantities such as $S_3{}'$ and $S_4{}'$, it is possible to correct not only the interference but also disturbances such as the laser wavelength shift and the spectral broadening.

## 5. Conclusion

We have developed a new gas analysis method using QCLs named IRLAM, which achieves high sensitivity and a high gas selectivity with a simple hardware configuration and a simple concentration calculation algorithm. The concept of the interference correction in IRLAM is similar to that in NDIR using pneumatic detectors and it is characterized by the extraction of the feature quantities from logarithmic gas absorption signals and by simultaneous linear equations with the extracted feature quantities. Furthermore, it is possible to correct other disturbances such as the spectral broadening due to the partial pressure changes of coexisting gases and the spectral shift due to the laser wavelength drift by extracting additional feature quantities concerning these disturbances. Since the extraction of the feature quantities efficiently reduces the number of variables for the concentration calculation, a computer with a high-performance CPU is unnecessary even in real-time measurements. It was demonstrated that the LOD is 2.0 ppb at the integration time of 1 s for CO gas measurement and that the interference by $N_2O$ can be completely eliminated with the IRLAM gas analyzer consisting of a 4.6 μm QCL, a 5 m path length Herriott cell with 40 ml internal volume and a thermopile as a detector. The IRLAM method allows construction of a compact, fast-response and robust gas analyzer by combining with the small-volume Herriott cell. Therefore, it can be expected to be applied particularly to fields that require portable and real-time measurements.

## Acknowledgments

## ORCID iD

Kyoji Shibuya ⓘ https://orcid.org/0000-0003-4004-3550

## References

[1] Hayes H V 1936 A new receiver of radiant energy *Rev. Sci. Instrum.* **7** 202–4

[2] Zahl H A and Golay J E 1946 Pneumatic heat detector *Rev. Sci. Instrum.* **17** 511–5

[3] Fastie W G and Pfund A H 1947 Selective infra-red gas analyzers *J. Opt. Soc. Am.* **37** 762–8

[4] Liston M D 1956 INSTRUMENTS United States 2924713

[5] Ishida K, Shimazaki T, Tanei F and Yagi T 1975 INFRARED GAS ANALYZER United States 3898462

[6] Werle P 1998 A review of recent advances in semiconductor laser based gas monitors *Spectrochim. Acta* A **54** 197–236

[7] Lackner M 2007 Tunable diode laser absorption spectroscopy (TDLAS) in the process industries - a review *Rev. Chem. Eng.* **23** 65–147

[8] Nasim H and Jamil Y 2013 Recent advancements in spectroscopy using tunable diode lasers *Laser Phys. Lett.* **10** 043001

[9] Bolshov M A, Kuritsyn Y A and Romanovskii Y V 2015 Tunable diode laser spectroscopy as a technique for combustion diagnostics *Spectrochim. Acta* B **106** 45–66

[10] Goldenstein C S, Spearrin R M, Jeries J B and Hanson R K 2017 Infrared laser-absorption sensing for combustion gases *Prog. Energy Combust. Sci.* **60** 132–76

[11] Faist J, Capasso F, Sivco D L, Sirtori C, Hutchinson A L and Cho A Y 1994 Quantum cascade laser *Science* **264** 553–6

[12] Kosterev A, Wysocki G, Bakhirkin Y, So S, Lewicki R, Fraser M, Tittel F and R F C 2008 Application of quantum cascade lasers to trace gas analysis *Appl. Phys.* B **90** 165–76

[13] Manne J, Lim A, Jäger W and Tulip J 2011 Wavelength modulation spectroscopy with a pulsed quantum cascade laser for the sensitive detection of acrylonitrile *Appl. Opt.* **50** E112–E118

[14] Cao Y, Sanchez N P, Jiang W, Griffin R J, Xie F, Hughes L C, Zah C and Tittel F K 2015 Simultaneous atmospheric nitrous oxide, methane and water vapor detection with a single continuous wave quantum cascade laser *Opt. Exp.* **23** 2121–32

[15] Moser H, Pölz W, Waclawek J P, Ofner J and Lendl B 2017 Implementation of a quantum cascade laser-based gas sensor prototype for sub-ppmv H2S measurements in a petrochemical process gas stream *Anal. Bioanal. Chem.* **409** 729–39

[16] Yu Y, Sanchez N P, Yi F, Zheng C, Ye W, Wu H, Griffin R J and Tittel F K 2017 Dual quantum cascade laser-based sensor for simultaneous NO and NO2 detection using a wavelength modulation-division multiplexing technique *Appl. Phys.* B **123** 164

[17] Hara K, Nakatani S, Montajir R, Nakamura H, Tanaka Y and Ukon J 2009 Development of nitrogen components analyzer utilizing quantum cascade laser *SAE Technical Paper* 2009-01-2743

[18] Montajir R 2010 Development of an ultra-low concentration N2O analyzer using quantum cascade laser (QCL) *SAE Technical Paper* 2010-01-1291

[19] Hangauer A, Chen J, Strzoda R and Amann M-C 2013 Multi-harmonic detection in wavelength modulation spectroscopy systems *Appl. Phys.* B **110** 177–85

[20] Liger V, Zybin A, Kuritsyn Y and Niemax K 1997 Diode-laser atomic-absorption spectroscopy by the double-beam-double-modulation technique *Spectrochim. Acta* B **52** 1125–38

[21] Zybin A V, Liger V V and Kuritsyn Y A 1999 Dynamic range improvement and background correction in diode laser atomic absorption spectrometry *Spectrochim. Acta* B **54** 613–9

[22] Klein A, Witzel O and Ebert V 2014 Rapid, time-division multiplexed, direct absorption- and wavelength modulation-spectroscopy *Sensors* **14** 21497–513

[23] Normand E, McCulloch M, Duxbury G and Langford N 2003 Fast, real-time spectrometer based on a pulsed quantum-cascade laser *Opt. Lett.* **28** 16–18

[24] McCulloch M T, Normand E L, Langford N and Duxbury G 2003 Highly sensitive detection of trace gases using the time-resolved frequency downchirp from pulsed quantum-cascade lasers *J. Opt. Soc. Am.* B **20** 1761–8

[25] Gordon I E *et al* 2017 The HITRAN2016 molecular spectroscopic database *J. Quant. Spectrosc. Radiat. Transfer* **203** 3–69

[26] Herriott D R and Schulte H J 1965 Folded optical delay lines *Appl. Opt.* **4** 883–9

[27] Sonnenfroh D M, Rawlins W T, Allen M G, Gmachl C, Capasso F, Hutchinson A L, Sivco D L, Baillargeon J N and Cho A Y 2001 Application of balanced detection to absorption measurements of trace gases with room-temperature, quasi-cw quantum-cascade lasers *Appl. Opt.* **40** 812–20

[28] Li J, Parchatka U, Königstedt R and Fischer H 2012 Real-time measurements of atmospheric CO using a continuous-wave room temperature quantum cascade laser based spectrometer *Opt. Exp.* **20** 7590–601